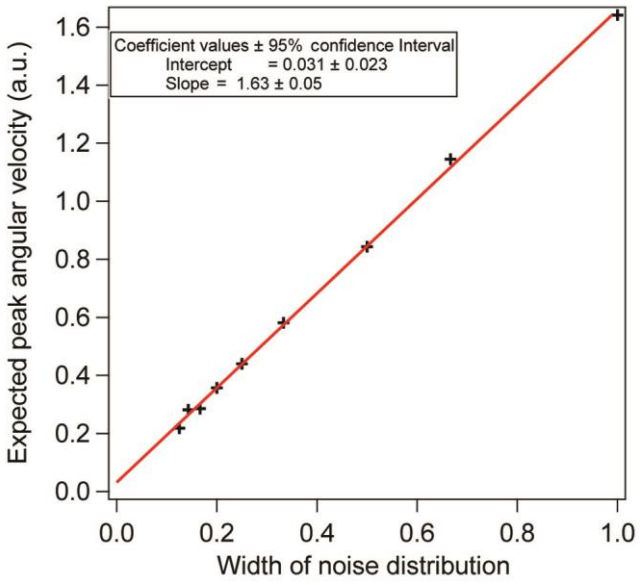

Figure 4. Plot indicating the expected peak angular velocity of particle as a function of width of the zero-mean Gaussian random noise α applied to the height of the potential barrier. The velocity is estimated as proportional to the square root of $(V(\alpha, \theta) - V(0, \theta))$, which is obtained using the peak of the histogram (like Figure 3) and substituting it in eq. (13). The angular velocity is linearly proportional to the width of the Gaussian noise.

This experiment can be used to ascertain the birefringence of small spherical particles of the dimension of a few micrometres accurately. The thermal noise complicates the method of detection of birefringence reported in Juodkazis *et al.*[13], which is only accurate to about 5%. A more accurate measurement would require accounting for the thermal random noise.

This communication described a new way of generating the washboard potential and producing directed continuous motion upon changing the barrier height randomly at the threshold. It also analysed, in two different ways, the velocity of the directed motion under specific amounts of random noise.

1. Reimann, P., Van den Broeck, C., Linke, H., Hanggi, P., Rubi, J. M. and Perez-Madrid, A., Giant acceleration of free diffusion by use of tilted periodic potentials. *Phys. Rev. Lett.*, 2001, **87**, 010602.
2. Pedaci, F., Huang, Z., van Oene, M., Barland, S. and Dekkar, N. H., Excitable particles in an optical torque wrench. *Nat. Phys.*, 2011, **7**, 259–264.
3. Tatarkova, S. A., Sibbett, W. and Dholakia, K., Brownian particle in an optical potential of the washboard type. *Phys. Rev. Lett.*, 2003, **91**, 038101.
4. Faucheux, L. P., Bourdieu, L. S., Kaplan, P. D. and Libchaber, A. J., Optical thermal ratchet. *Phys. Rev. Lett.*, 1995, **74**, 1504.
5. Sanchez-Palencia, L., Carminati, F.-R., Schiavoni, M., Renzoni, F. and Grynberg, G., Brillouin propagation modes in optical lattices: interpretation in terms of nonconventional stochastic resonance. *Phys. Rev. Lett.*, 2002, **88**, 133903.
6. Devoret, M. H., Martinis, J. M., Esteve, D. and Clarke, J., Resonant activation from the zero-voltage state of a current-biased Josephson junction. *Phys. Rev. Lett.*, 1984, **53**, 1260.
7. Chen, Y.-C. and Lebowitz, J. L., Quantum particle in a washboard potential. II. Nonlinear mobility and the Josephson junction. *Phys. Rev. B*, 1992, **46**, 10751–10762.
8. Freise, M. E. J., Nieminen, T. A., Heckenberg, N. R. and Rubinsztein-Dunlop, H., Optical alignment and spinning of laser-trapped microscopic particles. *Nature*, 1998, **394**, 348–350.
9. Rowe, A. D., Leake, M. C., Morgan, H. and Berry, R. M., Rapid rotation of micron and submicron dielectric particles measured using optical tweezers. *J. Mod. Opt.*, 2003, **50**, 1539–1551.
10. Gosse, C. and Croquette, V., Magnetic tweezers: micromanipulation and force measurement at the molecular level. *Biophys. J.*, 2002, **82**, 3314–3329.
11. Roy, B., Bera, S. K. and Banerjee, A., Simultaneous detection of rotational and translational motion in optical tweezers by measurement of backscattered intensity. *Opt. Lett.*, 2014, **39**, 3316–3319.
12. Casado, J. M., Coherence resonance in a washboard potential. *Phys. Lett. A*, 2001, **291**, 82–86.
13. Juodkazis, S., Matsuo, S., Murazawa, N., Hasegawa, I. and Misawa, H., High-efficiency optical transfer of torque to a nematic liquid crystal droplet. *Appl. Phys. Lett.*, 2003, **82**, 4657–4659.

Received 22 September 2015; revised accepted 14 July 2016

doi: 10.18520/cs/v111/i12/2005-2008

Greener production of magnetic nanoparticles and their fabrication

Ashima Sharma and Kavita Tapadia*

Department of Chemistry, National Institute of Technology, Raipur 492 010, India

In the present study green synthesis of magnetic nanoparticles has been described. Green tea was used in the synthesis of these nanoparticles due to its reducing property. The surface of green tea–magnetic nanoparticles was modified with tetra ethyl orthosilicate for silica coating, and further silica-coated green tea–magnetic nanoparticles were amine-activated by (3-aminopropyl)triethoxysilane. The proposed work is simple and cost-effective. Characterization of the structure and composition of green synthesized magnetic nanoparticles was formulated by X-ray diffraction analysis, Fourier transform-infra red, scanning electron microscope, electron dispersive X-ray and high-resolution transmission electron microscope.

Keywords: Amine activation, fabrication, green synthesis, green tea, magnetic nanoparticles.

*For correspondence. (e-mail: ktapadia.chy@nitrr.ac.in)

IN recent years oxide nanoparticles (NPs) have an important place among nanomaterials due to their tremendous applications ranging from catalysis to electronics to biomedicine[1]. Among the huge range of oxide NPs, iron oxide NPs like magnetite and maghematite are unique due to their technological interest. Magnetic nanoparticles (MNPs) are a versatile group of materials that enable a broad range of technologies, many of which are dependent on their distinguished magnetic properties such as paramagnetism, diamagnetism, super-paramagnetism, ferromagnetism, ferrimagnetism, etc. Hence there is great interest in fabricating iron oxide-based magnetic materials. MNPs have importance in *in vitro* and *in vivo* biomedicine, including cellular therapy such as separation, cell labelling, purification, and targeted drug delivery, cancer therapy and magnetic resonance imaging (MRI)[2]. MNPs are mostly applied in biotechnology due to their physico-chemical and pharmacological properties, chemical composition, structure of the surface, magnetic behaviour, solubility and low toxicity[3]. Currently, various methods for synthesizing MNPs have been developed such as chemical precipitation method[4–6], thermal decomposition[7–9], surfactants[10], polyol process[11], sol–gel method[12], sonochemical synthesis[13,14], chemical methods[15], solvothermal synthesis[16], hydrothermal synthesis[17,18], mechano-chemical processing and emulsion technique[19,20]. The NPs so formed show specific properties. Now green nanotechnology is involved in the production of metal NPs, which minimizes or eliminates the production of toxic pollutants in the environment. The inactivated plant tissues[21], plant extracts[22] and other parts of living plants[23] are a modern option for the synthesis of metal NPs. Green synthesis makes use of eco-friendly, non-toxic and safe reagents[24].

The leaves of *Camellia sinensis* are put to minimal oxidation during processing to form green tea (GT)[25]. A cup of green tea has higher content of flavanoids and catechins compared to the same volume of other beverages considered healthy[26]. These act as antioxidants due to their reducing properties. Polyphenols are a prime choice for synthesis of metal NPs due to their reducing, capping and biodegradable properties[27].

There are various properties which make green tea popular in modern life, such as anticancer, antioxidant, reduced risks of heart stroke, glycemic control, etc. Hydroxyl (Polyphemus), carboxyl and amino functional groups present in its phytochemicals act as effective metal-reducing agents and capping agents to provide a robust coating on the metal NPs in a single step. Recently, green tea leaf has proved to be effective in the synthesis of iron NPs[28].

Usually surface of MNPs can be modified by an inert silica layer due to the strong affinity of the surface of MNPs towards silica. Aggregation in liquid as well as improvement of chemical stability can be activated by this coating[29]. This silanization method relies on the well-known Stober process[30]. The amino activity of silica-coated MNPs can be improved by (3-aminopropyl)-triethoxysilane (APTES) around the MNPs[31]. Organosilanes are bifunctional molecules containing a trialkoxy or trichlorosilane group which modifies the surface of NPs through the coating of aminopropylsilane groups (–O) 3Si–CH_2–CH_2–CH_2–NH_2 via formation of covalent bonds which are bound to the surface of MNPs[32]. Scheme 1 shows the preparation of MNPs. This green source for the synthesis of MNPs is more beneficial than contemporary physical or chemical processes, as green sources are found in abundance, are cheap and can be utilized conveniently. The end-products obtained from the green synthesis of MNPs are safe and discardable in the environment, and hence are applicable for the analysis of biomolecules.

Fe(III) nitrate nonahydrate ($Fe(NO_3)_3{\cdot}9H_2O$, ≥98%), Fe(II) sulphate ($FeSO_4{\cdot}2H_2O$, 99%), sodium hydroxide (≥97%) and ammonia solution GR (30%) were obtained from Merck, Mumbai, India. Green tea leaves were obtained from Rahimpur, India. Tetra ethyl orthosilicate (TEOS, ≥99%) was purchased from Merck, Darmstadt, Germany. Ethanol (99.9%), analytical reagent was purchased from Xilong Chemical Corporation, China. APTES (≥98%) was purchased from Sigma Aldrich Corporation, USA.

XRD measurements were made using an X-ray diffractometer (model PANalytical 3kW X'Pert Powder-Multifunctional instrument, Germany). Fourier transform infrared (FTIR) spectroscopic measurements were made (Thermo Nicolet, Avatar 370 model) in the spectral range 4000–400 cm^{-1} (Thermo Scientific, USA). High resolution transmission electron microscope (HRTEM) (JEM-2100, JOEL, Philips, Japan) and scanning electron microscopic (SEM) measurements were also made (JEOL Model JSM-6390LV, 10,000 Kv, 1 µm surface, GmbH, ZEISS, Germany). An LI-617 pH meter (Elico, Hyderabad, India) was used for pH measurements, and a Spinot

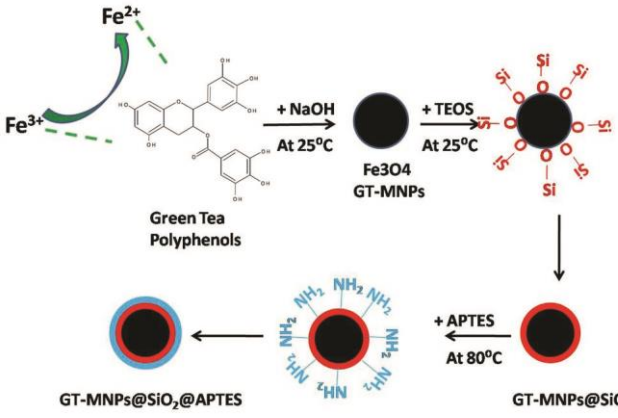

Scheme 1. Procedure for preparation of GT-MNPs (Fe_3O_4), GT-MNPs@SiO_2 and GT-MNPs@SiO_2@APTES.

magnetic stirrer with hot plate (Singhla Scientific Industry, Ambala Cant, India) was used for the preparation of MNPs.

In the proposed work green tea extract was prepared by boiling 50 g of green tea leaves in 500 ml double-distilled-water, until boiling temperature and then removing from the heating element. The extract was vacuum filtered after 1 h settlement.

For the preparation of green tea–magnetic nanoparticles (GT-MNPs), 0.1 M solution of Fe(III) and Fe(II) was made by dissolving 1 g of $Fe(NO_3)_3{\cdot}9H_2O$ and 0.469 g $Fe(SO_4){\cdot}2H_2O$ individually in 25 ml double-distilled water. The Fe(III) and Fe(II) solutions were mixed in 1 : 1 molar ratio with vigorous stirring. Green tea extract was added to the above mixture in 2 : 3 volume ratio with continuous stirring. Next 1 M NaOH was added to maintain a pH of 6. A black precipitate was obtained showing the formation of iron NPs, which were separated by applying an external magnetic field (Figure 1). Further evaporation of water was done to separate NPs, which were washed with ethanol (2–3 times). Then they were dried overnight in an oven.

For the fabrication of GT-MNPs surface using TEOS, Stober method was used with minor modifications in the preparation of core shell (Fe_3O_4@SiO_2) structure. MNPs (0.2 g) were dispersed in 20 ml of ethanol solution and sonicated for 15 min. Then 2 g TEOS in 25 ml ethanol and 3 ml of 30% NH_3 solution was added to the MNPs solution and sonicated at 16 W for 10 min. Vigorous stirring for 4 h under room temperature is an essential feature during this experiment. The final product so obtained was separated and washed 2–3 times with water, ethanol and acetone and dried at room temperature in vacuum.

For fabrication of silica coated GT-MNPs surface, GT-MNPs@SiO_2 (0.2 g) was dispersed in 45 ml of double-distilled water. The above solution was mixed with 5.0 ml of APTES. Thereafter, the solution was heated up to 80°C in a water bath for 3 h with continuous stirring. The end-product was dried overnight in an oven at 60°C after washing several times with water and ethanol.

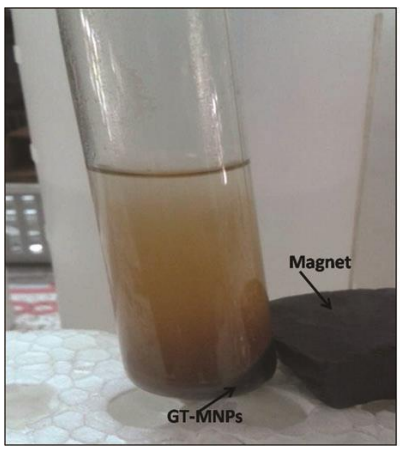

Figure 1. Magnetic nanoparticles in the presence of external magnet (magnetic field).

The characterization of bare and fabricated GT-MNPs (Fe_3O_4) was carried out respectively, by XRD, FTIR, SEM and TEM instruments. In FTIR analysis, the IR spectra were read in the 4000–400 cm^{-1} range using KBr pellets. Powder XRD scans of the samples were measured. Diffractograms were obtained using continuous scanning mode from 20° (2θ) to 70° (2θ) following a rate of 4° min^{-1}. In SEM, the topology of samples was recorded. HRTEM was used for the analysis of size and shape of MNPs. The samples for HRTEM analysis were suspended in ethanol in order to disperse the powder, and a drop of the sample was deposited on the vaccum-dried lacy copper grid. An accelerating voltage of 200 kV is required for TEM analysis.

Figure 2 *a*–*c* displays the XRD pattern of bare Fe_3O_4 (GT-MNPs), Fe_3O_4(GT-MNPs) @SiO_2MNPs and GT-MNPs@SiO_2 @APTES respectively. The characteristic peaks in the spectrum of bare GT-MNPs (Figure 2 *a*) agree well with the standard Fe_3O_4 (cubic phase) XRD spectrum. The peaks at $2\theta = 30.2°$, 35.6°, 43.2°, 57.3° and 62.9° resemble the (220), (311), (400), (422), (511) and (440) reflections respectively. Similar peaks are also observed in the spectra of GT-MNPs @SiO_2 (Figure 2 *b*) and GT-MNPs @SiO_2 @APTES (Figure 2 *c*) indicating that the crystalline structure and physical properties remain unchanged during fabrication of the surface of GT-MNPs, but the peaks remain unclear due to amorphous phase appearance after fabrication. The average crystallite size D was calculated using the Debye–Sherrer formula $D = K\lambda/(\beta\cos\theta)$, where K, λ, β and θ denote Sherrer constant, X-ray wavelength, peak width at half maximum and Bragg diffraction angle respectively. GT-MNPs of about 7.27 nm size were obtained using the above equation. Moreover, due to amorphous structure no crystalline structure was found in silica and APTES coatings.

SEM analysis in Figure S1 a (see Supplementary Information online) confirmed the cubic structure of GT-MNPs (Fe_3O_4). In Figure S1 *b* (see online) SEM analysis of GT-MNPs @SiO_2 shows spherical cluster formation due to SiO_2 coating. SEM analysis of GT-MNPs @SiO_2 @APTES shows a more dense structure (Figure S1 *c*, see Supplementary Information online). EDX spectra peak around 0.8, 0.9, 6.2 and 7.1 kV are related to the binding energies of Fe (Figure S2 *a*, see Supplementary Information online). Therefore the EDX spectra confirm the production of GT-MNPs (Fe_3O_4) without any impurities. The peaks around 0.8, 0.9, 6.2, 6.9, 2.1 kV in the EDX spectra (Figure S2 *b*, see Supplementary Information online) are connected to the binding energy of Fe and SiO_2 respectively. The peaks around 0.8, 0.9, 6.2, 6.9 kV (Figure S2 *c*, see Supplementary Information online) are related to the binding energy of Fe, and peak at 0.2 kV indicates

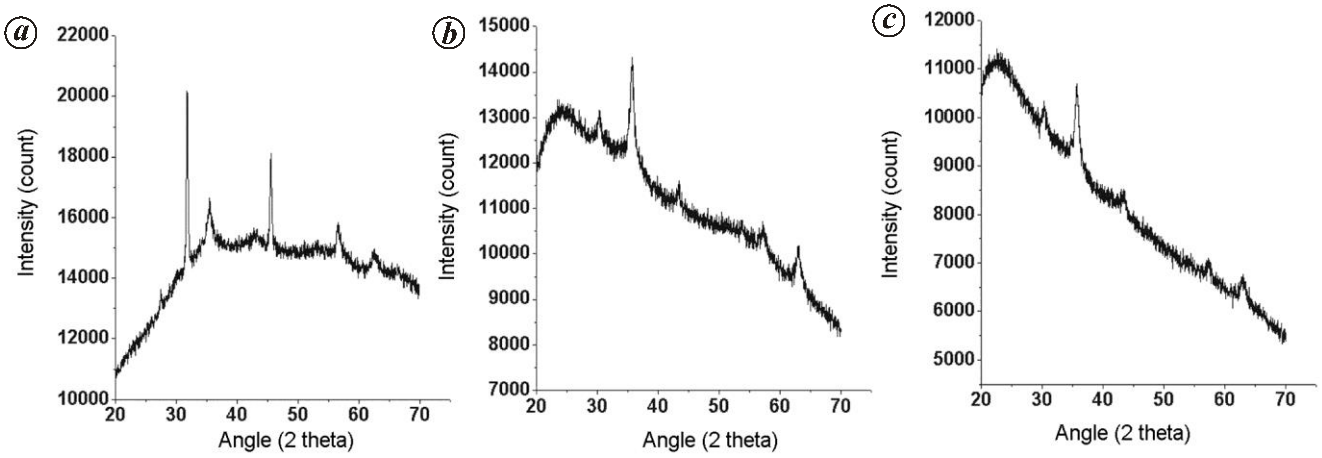

Figure 2. X-ray diffraction pattern of (***a***) GT-MNPs, (***b***) GT-MNPs@SiO_2 and (***c***) GT-MNPs@SiO_2@APTES (powder).

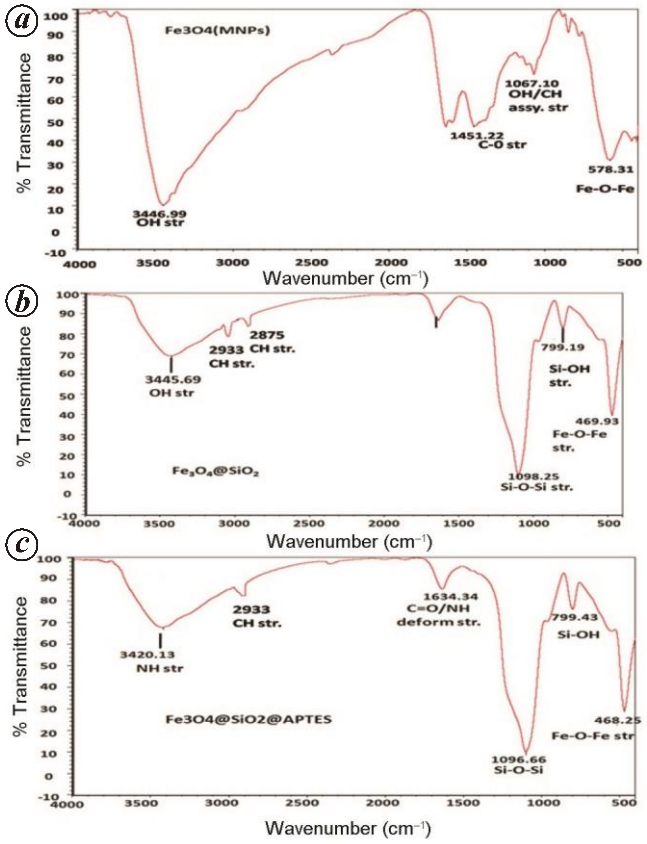

Figure 3. FTIR spectra of (***a***) GT-MNPs (Fe_3O_4), (***b***) GT-MNPs@SiO_2 and (***c***) GT-MNPs@SiO_2@APTES.

the binding energy of N, confirming the formation of GT-MNPs@SiO_2@APTES.

FTIR is a valuable tool for analysing the silanization process on the surface of GT-MNPs in order to confirm their fabrication. The FTIR spectra of bare GT-MNPs indicate Fe–O stretching, vibration at 578.31 cm^{-1} (Figure 3 *a*), 469.93 cm^{-1} (Figure 3 *b*) and 468.25 cm^{-1} (Figure 3 *c*), available in all three compounds. OH stretching, vibration at 3446.99 and 3445.69 cm^{-1} and O–H deformed vibration at 1632 cm^{-1} (Figure 3 *a* and *b*) show the coating of OH group on the surface of GT-MNPs. In Figure 3 *c* the band at 3420.15 cm^{-1} reveals the presence of stretching vibration band of the free amino groups present in APTES-coated GT-MNPs. As shown in Figure 3 *b* and *c*, formation of covalent bonds of Fe–O–Si is confirmed by the presence of Si–O stretching vibrations peaks at 1098 cm^{-1} during silanization process. The presence of anchored propyl group is confirmed by C–H stretching vibrations that appear at 2933 and 2875 cm^{-1} (Table 1).

HRTEM analysis of bare and fabricated GT-MNPs such as GT-MNPs@SiO_2 and GT-MNPs@SiO_2@APTES were approximately sphere-like with size ranging from 6 to 30 nm. In Figure 4 *a*, an aggregation in GT-MNPs can be seen. Histogram analysis was used to obtain the size of GT-MNPs as 7.5 nm. In Figure 4 *b*, due to silica coating the aggregation in MNPs is not visible. Histogram analysis revealed the size of GT-MNPs@SiO_2 to be 11.75 nm. Figure 4 *c* shows that the thick coating of APTES on the surface of GT-MNPs@SiO_2 causes complete separation of NPs, therefore the size of GT-MNPs@SiO_2@APTES is a critical factor to be determined.

In the present study, an eco-friendly production of MNPs was achieved using green tea and fabricated with silica and APTES. The synthesized products (GT-MNPs, GT-MNPs@SiO_2 and GT-MNPs@SiO_2@APTES) were analysed using XRD, SEM, TEM and FTIR with good results. XRD and SEM analysis confirmed the cubic nature and shape of GT-MNPs. FTIR revealed that the MNPs has great affinity towards silica and NH_2, during the fabrication process. TEM analysis provided the average size of GT-MNPs to be 7.5 nm. Thus the fabrication process

Table 1. FTIR analysis of bare Fe_3O_4 (GT-MNPs), Fe_3O_4 (GT-MNPs)@SiO_2 and Fe_3O_4(GT-MNPs)@SiO_2@ APTES

Bond	Bare Fe_3O_4(GT-MNPs) (cm^{-1})	Fe_3O_4(GT-MNPs)@SiO_2 (cm^{-1})	Fe_3O_4(GT-MNPs)@SiO_2@APTES (cm^{-1})
Fe–O	578.31	469.93	468.25
(HO–H)	3446.99	3445.69	
Si–OH str.		799.43	845.76
Si–O–Si		1098.25	1098.55
N–H			3420.15, 1634.34
HC–H		2933, 2875.13	2933

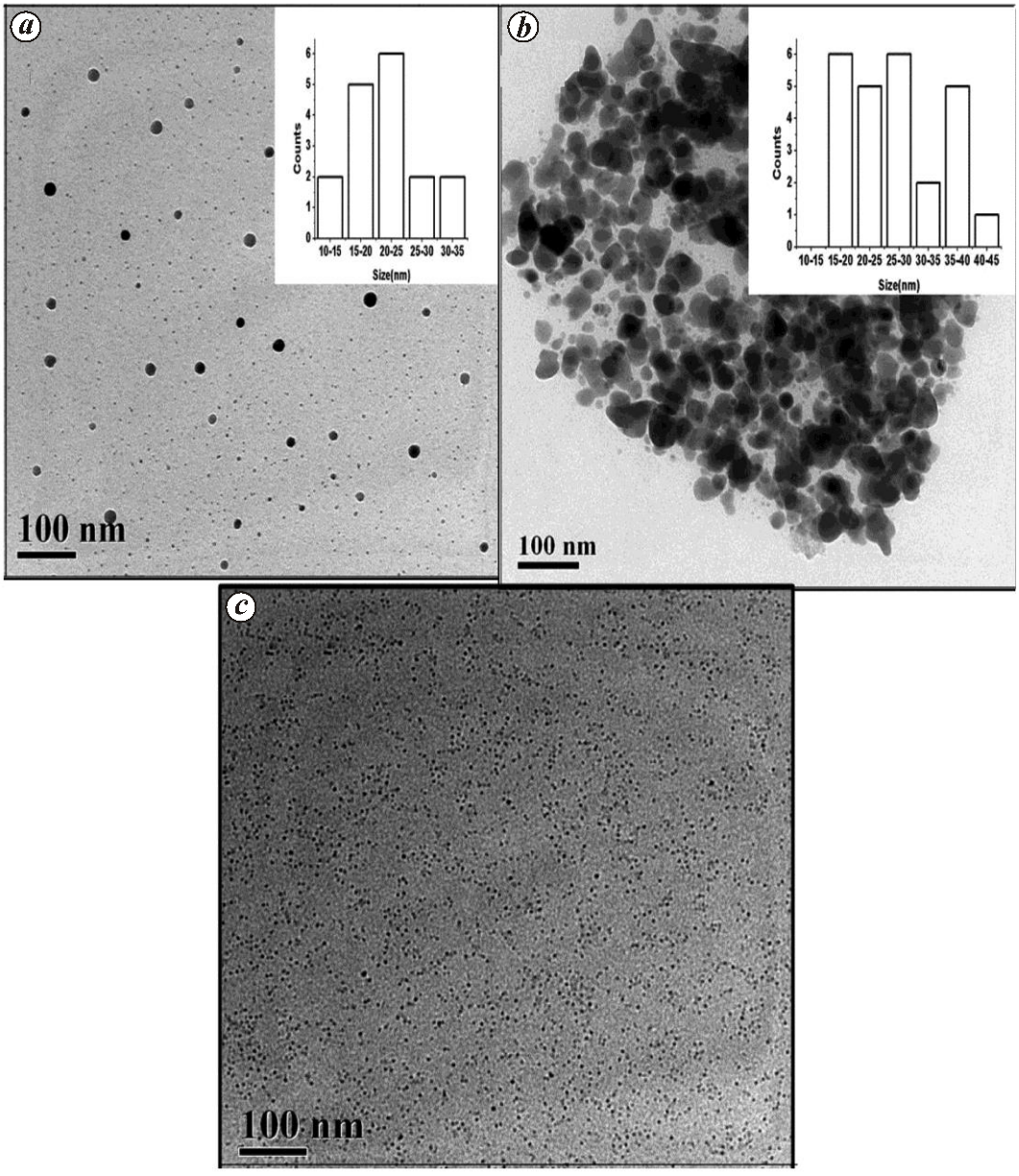

Figure 4. HRTEM images of (***a***) GT-MNPs, (***b***) GT-MNPs@SiO_2 and (***c***) GT-MNPs@SiO_2@APTES.

avoided the aggregation of GT-MNPs and is responsible for stability of GT-MNPs. After fabrication, the bio-compability of GT-MNPs was improved. It can be used in various biomedical and bioanalytical applications.

1. Fernandez, G. M., Martinez, A. A., Hanson, J. C. and Rodriguez, J. A., Nanostructure oxides in chemistry: its characterization and properties. *Chem. Rev.*, 2004, **104**, 4063–4104.
2. Feng, B., Hong, R. Y., Wang, L. S., Guo, L. and Li, H. Z., Synthesis of Fe_3O_4/APTES/PEG diacid functionalized magnetic nanoparticles for MR imaging. *Colloids Surf. A*, 2008, **328**, 52–59.
3. Khosroshahi, M. E. and Ghazanfari, L., Preparation and characterization of silica-coated iron-oxide bionanoparticles under N_2 gas. *Physica E*, 2010, **42**, 1824–1829.
4. Maity, D. *et al.*, Facile synthesis of water-stable magnetite nanoparticles for clinical MRI and magnetic hyperthermia applications. *Nanomedicine*, 2010, **5**, 1571–1584.
5. Yu, W. T., Zhang, T., Zhang, J., Qiao, X., Yang, L. and Liu, Y., The synthesis of octahedral nanoparticles of magnetite. *Mater. Lett.*, 2006, **60**, 2998–3001.
6. Zhu, Y. and Wu, Q., Synthesis of magnetite nanoparticles by precipitation with forced mixing. *J. Nanopart. Res.*, 1999, **1**, 393–396.
7. El, G. H., Zidan, H. M., Khalil, M. M. H. and Ismail, M. I. M., Synthesis and some physical properties of magnetite (Fe_3O_4) nanoparticles. *Int. J. Electrochem. Sci.*, 2012, **7**, 5734–5745.
8. Maity, D., Kale, S. N., Kaul, G. R., Xue, J. M. and Ding, J., Studies of magnetite nanoparticles synthesized by thermal decomposition of iron(III) acetylacetonate in triethylene glycol. *J. Magn. & Magn. Mater.*, 2009, **321**, 3093–3098.
9. Woo, K., Hong, J., Choi, S., Lee, H. W., Ahn, J. P., Kim, C. S. and Lee, S. W., Easy synthesis of magnetite properties of iron oxide nanoparticles. *Chem. Mater.*, 2004, **16**, 2814–2818.
10. Rockenberger, J., Scher, E. C. and Alivisatos, A. P., A new nonhydrolytic single-precursor approach to surfactant-capped nanocrystals of transition metal oxides. *J. Am. Chem. Soc.*, 1999, **121**, 11595–11596.
11. Cai, W. and Wan, J., Facile synthesis of superparamagnetic magnetite nanoparticles in liquid polyols. *J. Colloid Interface Sci.*, 2007, **305**, 366–370.
12. Xu, J. *et al.*, Preparation and magnetic properties of magnetite nanoparticles by sol–gel method. *J. Magn. Magn. Mater.*, 2007, **309**, 307–311.
13. Vijayakumar, R., Koltypin, Y., Felner, I. and Gedanken, A., Sonochemical synthesis and characterization of pure nanometer-sized Fe_3O_4 particles. *Mater. Sci. Eng. A*, 2000, **286**, 101–105.
14. Dang, F., Enomoto, N., Hpjo, J. and Enpuku, K., Sonochemical synthesis of monodispersedmagnetite nanoparticles by using an ethanol–water mixed solvent. *Ultrasonics Sonochem.*, 2009, **16**, 649–654.
15. Pei, W., Kumada, H., Saito, H. and Ishio, S., Study on magnetite nanoparticles synthesized by chemical method. *J. Magn. Magn. Mater.*, 2007, **310**, 2375–2377.
16. Zhang, W., Shen, F. and Hong, R., Solvothermal synthesis of magnetite Fe_3O_4 microparticles via self-assembly of Fe_3O_4 nanoparticles. *Particuology*, 2011, **9**, 179–186.
17. Mizutani, N., Iwasaki, T., Watano, S., Yanagida, T., Tanaka, H. and Kawai, T., Effect of ferrous/ferric ion molar ratio on reaction mechanism for hydrothermal synthesis of magnetite nanoparticles. *Bull. Mater. Sci.*, 2008, **31**, 713–717.
18. Han, C., Cai, W., Tang, W., Wang, G. and Liang, C., Protein assisted hydrothermal synthesis of ultrafine magnetite. *J. Mater. Chem.*, 2011, **21**, 1188–1196.
19. Bretcanu, O., Verné, E., Coisson, M., Tiberto, P. and Allia, P., Magnetic properties of the ferrimagnetic glass-ceramics for hyperthermia. *J. Magn. Magn. Mater.*, 2006, **305**, 529–533.
20. Jun, Y. W. *et al.*, Nanoscale size effect of magnetic nanocrystals and their utilization for cancer diagnosis resonance. *J. Am. Chem. Soc.*, 2005, **127**, 5732–5733.
21. Padil, V. V. and Cerník, M., Green synthesis of copper oxide nanoparticles using gum karaya as abiotemplate and their antibacterial application. *Int. J. Nanomed.*, 2013, **8**, 889–898.
22. Shameli, K., Ahmad, M. B., Zamanian, A., Sangpour, P., Shabanzadeh, P., Abdollahi. Y. and Zargar, M., Green biosynthesis of silver nanoparticles using *Curcuma longa* tuber powder. *Int. J. Nanomed.*, 2012, **7**, 5603–5610.
23. Parsons, J. G., Peralta, V. J. R. and Gardea, T. J. L., Use of plants in biotechnology: synthesis of metal nanoparticles by inactivated plant tissues, plant extracts, and living plants. *Dev. Environ. Sci.*, 2007, **5**, 463–485.
24. Salam, H. A., Rajiv, P., Kamaraj, M., Jagadeeswaran, P., Gunalan, S. and Sivaraj, R., Plants: green route for nanoparticle synthesis. *Int. J. Biol. Sci.*, 2012, **1**, 85–90.
25. Khan, N. and Mukhtar, H., Tea and health: studies in humans. *Curr. Pharma. Design* (*Lit. Rev.*), 2013, **19**(34), 6141–6147.
26. USDA Database for the Flavonoid Content of Selected Foods, Release 2.1, 2007.
27. Nadagouda, M. N., Castle, A. B., Murdock, R. C., Hussain, S. M. and Varma, R. S., *In vitro* biocompatibility of nanoscale zerovalent iron particles (NZVI) synthesized using tea polyphenols. *Green Chem.*, 2010, **12**, 114–122.
28. Hoag, G., Collins, J., Holcomb, J., Hoag, J., Nadagouda, M. and Varma, R., Degradation of bromothylmol blue by 'greener' nanoscale zero-valent iron synthesized using tea polyphenols. *J. Mater. Chem.*, 2009, **19**, 8671–8677.
29. Sun, Y. *et al.*, An improved way to prepare superparamagnetic magnetite–silica core shell nanoparticles for possible biological application. *J. Magn. & Magn. Mater.*, 2005, **285**, 65–70.
30. Zhang, L., Liu, B. and Dong, S., Bifunctional nanostructure of magnetic core luminescent shell and its application as solid-state electro chemiluminescence sensor material. *J. Phys. Chem. B*, 2007, **111**, 10448–10452.
31. Yamaura, M., Camilo, R. L., Sampaio, L. C., Macedo, M. A., Nakamura, M. and Toma, H. E., Preparation and characterization of (3-aminopropyl) triethoxysilane coated magnetite nanoparticles. *J. Magn. & Magn. Mater.*, 2004, **279**, 210–217.
32. Park, J. O., Rhee, K. Y. and Park, S. J., Thermo mechanical properties of unsaturated polymer toughened epoxy siliconized iron(III) oxide nanocomposites. *Appl. Surf. Sci*., 2010, **256**, 6945–6950.

ACKNOWLEDGEMENTS. We thank the National Institute of Technology, Raipur, and the Indian Institute of Technology. Kharagpur for providing the necessary facilities for lab work and analysis.

Received 7 August 2015; revised accepted 26 May 2016

doi: 10.18520/cs/v111/i12/2008-2013